Cell Reports
Physical Science

CellPress

Article

Carbon Dioxide Capture Using an Electrochemically Driven Proton Concentration Process

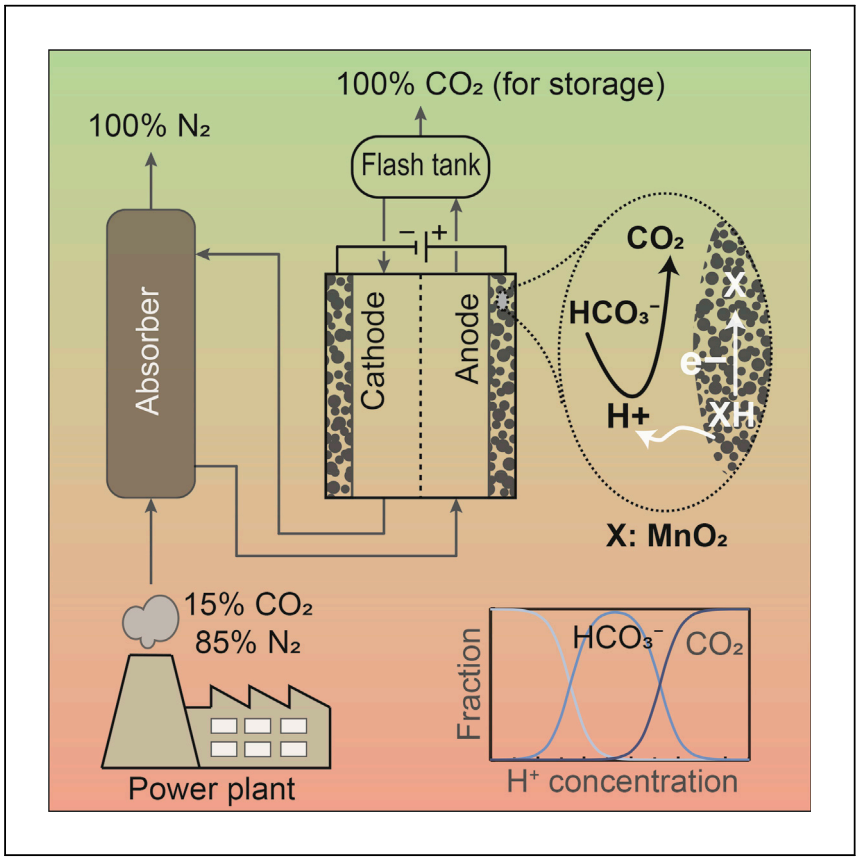

Rahimi et al. introduce an electrochemically driven proton concentration process for CO_2 capture. MnO_2 electrodes that intercalate or deintercalate protons are used to take advantage of the pH sensitivity of the CO_2 hydration equilibrium. Intercalation of proton ions at the cathode drives the capture of CO_2 as either HCO_3^- or CO_3^{2-}, while release occurs at the anode where deintercalation of the proton from the electrode matrix results in increasing the proton concentration, leading to regeneration of free CO_2.

Mohammad Rahimi, Giulia Catalini, Subrahmaniam Hariharan, Miao Wang, Monica Puccini, T. Alan Hatton

tahatton@mit.edu

HIGHLIGHTS

An electrochemically driven proton concentration process is proposed to capture CO_2

A comprehensive thermodynamic model is developed to evaluate the proposed process

The electrochemical work required to desorb CO_2 is estimated to be 33.2 kJe/mol CO_2

The generated current is effectively translated into proton concentration change

Rahimi et al., Cell Reports Physical Science 1, 100033
April 22, 2020
https://doi.org/10.1016/j.xcrp.2020.100033

Please cite this article in press as: Rahimi et al., Carbon Dioxide Capture Using an Electrochemically Driven Proton Concentration Process, Cell Reports Physical Science (2020), https://doi.org/10.1016/j.xcrp.2020.100033

Cell Reports
Physical Science

CellPress

Article

Carbon Dioxide Capture Using an Electrochemically Driven Proton Concentration Process

Mohammad Rahimi,[1] Giulia Catalini,[1,2] Subrahmaniam Hariharan,[1] Miao Wang,[1] Monica Puccini,[2] and T. Alan Hatton[1,3,*]

SUMMARY

The development of sustainable CO_2 capture technologies is critical to address issues associated with global warming. In this context, the concept of an electrochemically driven proton concentration process is developed for the capture of CO_2 based on modulation of the proton concentration in an electrochemical cell by a proton intercalating MnO_2 electrode. The pH sensitivity of CO_2 hydration is leveraged such that CO_2 is absorbed as bicarbonate and carbonate ions at high pH values and desorbed as gas at low pH values. The electrochemical work requirement for the proposed proton concentration process to desorb CO_2 captured from a flue gas stream is estimated to be 33.2 kJe/mol CO_2, suggesting that this process is competitive with other similar electrochemical-based approaches. The experimental results show that the generated current in a symmetrical electrochemical cell with fabricated electrodes is effectively translated into proton intercalation/deintercalation reactions through reversible cycles, resulting in modulated proton concentrations.

INTRODUCTION

Over the past few decades, atmospheric carbon dioxide (CO_2) concentrations have risen steeply; in May 2019, atmospheric CO_2 reached 415 ppm, a level higher than any reached in >800,000 years.[1] With increasing evidence of global warming and its correlation with CO_2 emissions, the development of cost-effective, large-scale, and efficient CO_2 capture technologies is critical.[2,3] State-of-the-art technologies for CO_2 capture involve thermal cycles in which a nucleophilic agent captures CO_2 from impure gas streams (e.g., flue gas), followed by a thermal stripping process in which pure CO_2 is released and the nucleophilic agent is regenerated.[4,5] The most developed capture system based on this method uses an amine absorbent such as monoethanolamine, which acts as a nucleophile, reacting with CO_2 at the electrophilic carbon center to form a carbamate.[4,6] Despite their widespread use, amine-based thermal scrubbing processes face several challenges that have slowed their deployment on very large scales. These challenges include the high energy requirement for regeneration,[4,5,7] the degradation of amines at high temperature,[5,8] corrosion issues,[9–11] and high operational costs.[12] As an alternative to amines in the thermal scrubbing process, potassium carbonate (K_2CO_3) has been widely investigated as an absorbent. It offers several advantages, including a high capacity for CO_2 absorption, a low degradation rate, ease of regeneration, low cost and toxicity, and low corrosiveness.[7,13–15] The major disadvantage of K_2CO_3 is its low rate of reaction with CO_2, resulting in poor performance of the absorber stage.[7,16] Efforts to address the challenges faced by thermal scrubbing processes are ongoing.

[1]Department of Chemical Engineering, Massachusetts Institute of Technology, Cambridge, MA 02139, USA

[2]Department of Civil and Industrial Engineering, University of Pisa, Largo Lucio Lazzarino 2, 561226 Pisa, Italy

[3]Lead Contact

*Correspondence: tahatton@mit.edu

https://doi.org/10.1016/j.xcrp.2020.100033

Cell Reports
Physical Science

Alternative approaches based on electrochemistry have drawn increasing attention in recent years. Early efforts in using electrochemistry for CO_2 capture date to the late 1960s, when a molten carbonate fuel cell was developed to remove CO_2 from complex gas streams.[17] Another approach used the electrochemical reduction of organic redox compounds to generate nucleophiles that could bind to the electrophilic carbon center in CO_2, resulting in the selective capture of CO_2 from a gas mixture.[18–21] CO_2 can also be captured using electrochemically controlled pH swings as the primary driver. These approaches take advantage of the pH sensitivity of the thermodynamic equilibrium of CO_2. In this context, two different processes, a bipolar membrane electrodialysis[22] and a redox-mediated pH swing,[23] have previously been introduced.

Two recently developed electrochemical systems to capture CO_2 are electrochemically mediated amine regeneration (EMAR)[24] and membrane capacitive deionization (MCDI).[25] In the EMAR process, a CO_2-rich amine stream from the absorber is introduced to an electrochemical cell in which copper ions are electrochemically generated from a copper plate anode to drive the dissociation of amine and CO_2 toward CO_2 desorption. Once the gas is flashed off, the CO_2 lean stream is regenerated via the electrochemical plating of copper on the cathode from the copper-amine complex.[24,26] The EMAR approach offers several advantages over thermally driven amine-based processes, including operation at low temperature (thereby minimizing thermal amine degradation) and the ability to desorb CO_2 at moderate pressures, which minimizes the downstream compression costs for CO_2 storage.[27] Recently, MCDI was adapted to capture CO_2 in the form of HCO_3^- and CO_3^{2-}, using deionized water as the solvent.[25] In this system, HCO_3^- and CO_3^{2-} ions are captured in the electrical double layer established at a carbon-based anode surface. CO_2 was successfully desorbed from a gas mixture containing various concentrations of CO_2 through energy-efficient cycles. Although MCDI is still in the early stages of development, such systems may represent an opportunity to attract expertise from the field of capacitive deionization into carbon capture.

In this study, we introduce an electrochemical approach with electrodes that intercalate/deintercalate protons to take advantage of the pH sensitivity of the CO_2 hydration equilibrium. The process scheme consists of three chemical or electrochemical transitions that take place in an absorber, an anode, and a cathode. The absorber is analogous to those used in thermal scrubbing systems, but the absorbent capture mechanism is based on the hydration of CO_2 (i.e., when using K_2CO_3) rather than carbamate formation (i.e., when using a primary or secondary amine); hence, CO_2 is absorbed as bicarbonate (HCO_3^-) and carbonate (CO_3^{2-}) (Equations 1 and 2). A stream with high CO_2 loading is then sent to the anode compartment of an electrochemical cell where deintercalation of protons from an electrode (denoted "X") to the solution (Equation 3; the oxidation reaction) results in a local decrease in the solution pH, which shifts the $CO_{2\,(aq)}/HCO_{3\,(aq)}^-/CO_{3\,(aq)}^{2-}$ equilibrium toward CO_2 formation. Potassium chloride (KCl) is used as the background electrolyte, and Cl^- ion transfer through an anion exchange membrane ensures charge neutrality. The desorbed CO_2 is separated through a flash tank located after the anode compartment. To regenerate the absorbent, the stream is sent to the cathode compartment, where the solution pH is increased as a result of proton intercalation during the reduction reaction (Equation 3). The regenerated solution with high pH is then sent to the absorber column for further absorption. Therefore, CO_2 capture and release can be achieved by chemical absorption, followed by electrochemical regeneration of the absorbent through a proton concentration process. To prevent a complete saturation of the cathode with proton and depletion of the anode, the

Please cite this article in press as: Rahimi et al., Carbon Dioxide Capture Using an Electrochemically Driven Proton Concentration Process, Cell Reports Physical Science (2020), https://doi.org/10.1016/j.xcrp.2020.100033

Cell Reports
Physical Science

CellPress

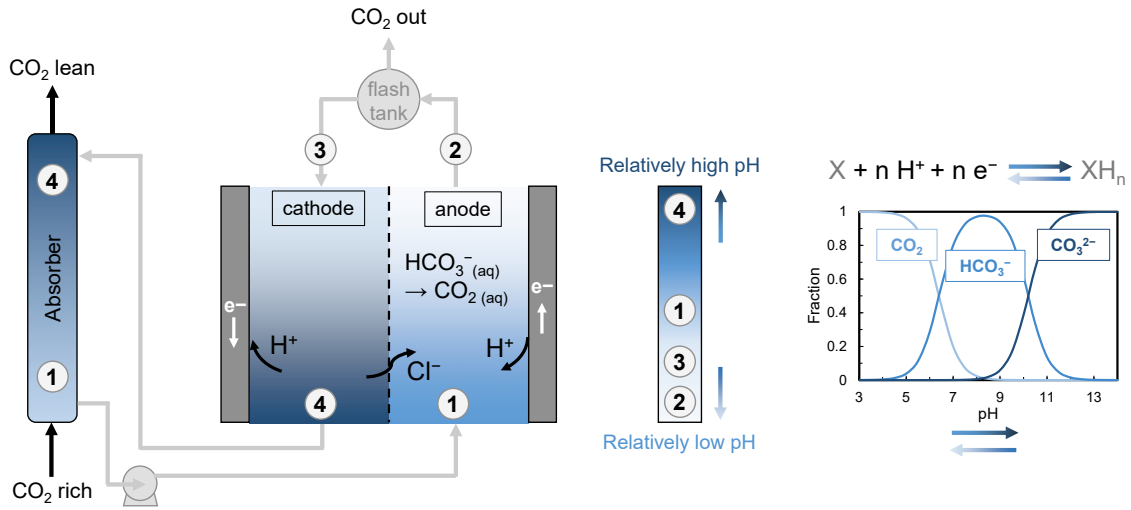

Figure 1. Schematic of the Proposed Proton Concentration Process for CO_2 Capture

In the absorber, CO_2 is selectively absorbed by a K_2CO_3 absorbent, resulting in a decrease in the solution pH (i.e., 4 → 1). The solution is then introduced to the anode compartment of an electrochemical cell, where proton deintercalation from the electrode (denoted "X") shifts the $CO_{2\,(aq)}$/ $HCO_3^{-}{}_{(aq)}$/ $CO_3^{2-}{}_{(aq)}$ equilibrium toward CO_2 formation (i.e., 1 → 2), followed by gas separation through a flash tank (i.e., 2 → 3). Subsequently, the absorbent is regenerated in the cathode compartment, where proton intercalation occurs (i.e., 3 → 4). KCl was used as the background electrolyte, and Cl^- ions transfer through an anion exchange membrane was considered for the charge neutrality. The process takes advantage of the pH sensitivity of the thermodynamic equilibrium of CO_2 (right panel).

electrode polarity and the fluidic paths of the electrochemical cell must be switched periodically. A similar polarity change strategy was implemented in our previous experimental setup for electrochemically mediated amine regeneration with copper electrodes to prevent a complete corrosion of the anode.[28] Figure 1 shows a schematic of the process, including an absorber, an electrochemical cell as the desorber, and a flash tank to separate the desorbed CO_2.

$$CO_{2\,(aq)} + H_2O + K_2CO_3 \rightleftharpoons 2KHCO_{3\,(aq)} \quad (1)$$

$$HCO_{3^-(aq)} \rightleftharpoons CO_{3^{2-}(aq)} + H^+_{(aq)} \quad (2)$$

$$X_{(s)} + n\,H^+_{(aq)} + n\,e^- \rightleftharpoons XH_{n\,(s)} (n,\ \text{the number of electrons transferred}). \quad (3)$$

The primary goal of this investigation was to estimate the energetics of such an approach by constructing a thermodynamic model that predicts the process parameters, as well as to introduce an electrode that could host protons to electrochemically modulate proton concentration. In this context, we develop a detailed thermodynamic model of this proton concentration process, including a rigorous speciation and activity coefficient description, to predict the (electro)chemical parameters that are later used to estimate the energetics of the electrochemical cell. The model is validated by several experimental measurements. To electrochemically swing the proton concentration, manganese dioxide (MnO_2)-based electrodes that could effectively host protons (i.e., intercalation) during reduction and release these ions (i.e., deintercalation) during oxidation were developed. MnO_2 is a low-cost, Earth-abundant, and environmentally friendly electrode material with high theoretical capacitance (~1,100 F g^{-1}).[29,30] MnO_2 electrodes with capacities close to the theoretical value can be obtained using advanced fabrication techniques, which is beyond the scope of this investigation. Rather, we focus on demonstrating that this material could be used in an electrode to effectively host and release proton

Please cite this article in press as: Rahimi et al., Carbon Dioxide Capture Using an Electrochemically Driven Proton Concentration Process, Cell Reports Physical Science (2020), https://doi.org/10.1016/j.xcrp.2020.100033

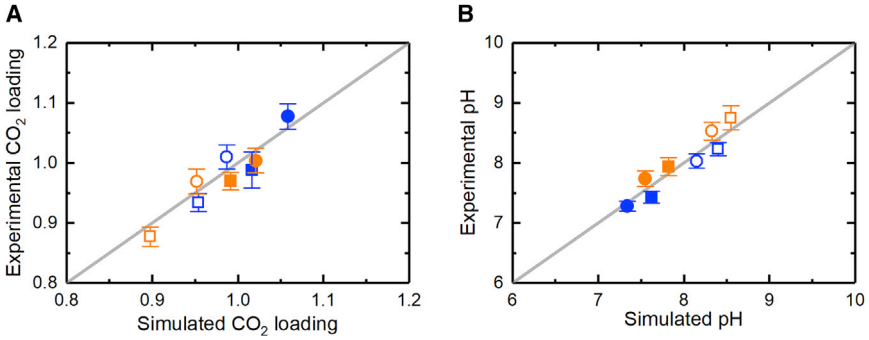

Figure 2. Thermodynamic Model Verification for the Absorption Process

(A and B) Comparing the simulated values of (A) CO_2 loading and (B) solution pH with their corresponding experimental measurements. The experiments were performed at various combinations of K_2CO_3 absorbent concentration (0.5 mol kg^{-1}, circles; 1 mol kg^{-1}, squares), gas compositions (15 mol% CO_2 and 85 mol% N_2, open symbols; 100 mol% CO_2, filled symbols), and temperatures (23°C, blue symbols; 50°C, orange symbols). Error bars represent SDs of the experimental CO_2 loading and pH values of three independent replicates.

ions through reversible intercalation/deintercalation cycles. The MnO_2 electrode potentials were previously shown to be responsive when exposed to solutions of different pH and have been used as electrodes to generate electrical power for such a system. An open circuit potential of ~60 mV per 1 unit of pH difference between anolyte and catholyte (i.e., d*E*/dpH = 60 mV) was obtained.[31,32] In contrast, in the present study, we use these electrodes to generate a pH difference by applying electrical power. The fabricated electrodes are characterized to evaluate their chemical state and capacitance properties. The electrochemical responsiveness of the solution pH toward the polarization of MnO_2 electrodes was also investigated.

RESULTS

Thermodynamic Model Verification

The developed thermodynamic speciation and activity coefficient models were validated for the absorption and desorption processes. For absorption, experiments were performed with 2 K_2CO_3 absorbent concentrations (0.5 or 1 mol kg^{-1}) at different temperatures (23°C or 50°C) under various gas compositions (15 mol% CO_2, 85 mol% nitrogen [N_2]; 100 mol% CO_2). For each experiment, the CO_2 capacity and absorbent pH were measured, and the experimental values were compared with those of the simulation (Figure 2). The simulated CO_2 loadings and pH were in good agreement with the experimental values, confirming that the thermodynamic speciation and activity coefficient models provided accurate representations of these solution compositions.

The model was also validated for the CO_2 desorption process. A solution of 0.5 mol kg^{-1} K_2CO_3 was saturated with a gas stream containing 15 mol% CO_2 and 85 mol% N_2 at 50°C, similar to the composition of flue gas. To desorb CO_2, various concentrations of HCl were added to the solution to mimic desorption in the electrochemical cell, in which H^+ ions are introduced by deintercalation from the electrode and Cl^- ions are transferred from the cathode to the anode compartment through the anion-exchange membrane. Similar to the absorption process, CO_2 loading and pH were measured for each added HCl concentration in the desorption process; the experimental results matched well with the simulated values (Figure 3). The solution pH was not affected much at low concentrations of HCl, mainly due to the high buffer capacity of the solution, which is derived from the

Cell Reports
Physical Science

CellPress

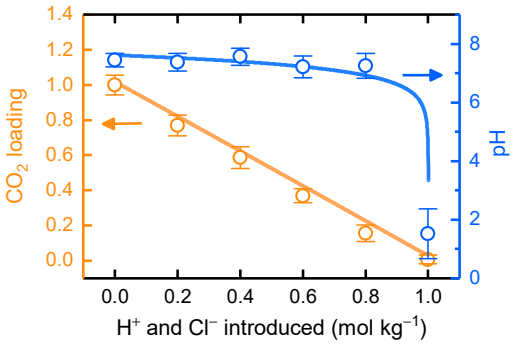

Figure 3. Thermodynamic Model Verification for the Desorption Process

The simulated results of CO_2 loading (orange line) and solution pH (blue line) were compared with their corresponding experimental values (circles) at various added HCl concentrations. A solution of 0.5 mol kg^{-1} K_2CO_3 saturated with 15 mol% CO_2 and 85 mol% N_2 at 50°C was used. Error bars represent SDs of the experimental CO_2 loading and pH values of three independent replicates.

$CO_2/HCO_3^-/CO_3^{2-}$ buffer system. However, CO_2 loading decreased linearly with the introduction of proton ions, resulting in a 1:1 ratio between the moles of CO_2 desorbed to the moles of proton introduced. This means that despite the high buffering capacity of the solution, which prevents a pH swing, CO_2 can be effectively desorbed by proton introduction (which, in the electrochemical cell, comes from electrode deintercalation).

For both the absorption and desorption measurements, experimental errors were likely due to CO_2 titration inaccuracies, experimental uncertainties of pH measurements at 50°C (including calibration at 50°C), and the limitations of the activity coefficient model, which is accurate only up to an ionic strength of 1 mol kg^{-1}. Overall, the thermodynamic model developed here predicted the thermodynamic properties of the system with good accuracy and could be used further to estimate the electrochemical work needed to desorb CO_2.

Thermodynamic Cycle and Electrochemical Energetics

The electrochemical behavior of the system was evaluated through its electrochemical thermodynamic cycle constructed based on the Nernst equation at different chloride loadings. As an example, we considered the capture of CO_2 from a flue gas stream with 15 mol% CO_2 and 85 mol% N_2 by 0.5 mol kg^{-1} K_2CO_3 absorbent and 0.5 mol kg^{-1} KCl as the background electrolyte at 50°C. We assumed an electrode with one electron transfer (n = 1) and an intercalation efficiency of 0.7, which is the case for MnO_2 electrodes reported in previous investigations.[31,33] For this operating condition, the half-cell equilibrium potentials (i.e., E_{ox} and E_{red}) as a function of chloride loading were calculated with the results illustrated in Figure 4. Point 1 corresponds to the stream entering the anode compartment, which was equilibrated with 15 mol% CO_2 and 85 mol% N_2 in the absorber. The stream was then passed through the anode compartment (i.e., 1 → 2), where the proton concentration (and, equivalently, the chloride loading) was modulated by applying an electrical potential. The potential profile during this process (E_{ox}) shows a sharp increase, followed by a nearly linear trend as chloride loading increases across the cell. The initial ramping of the potential could be related to the release of CO_2 that remains in solution at partial pressures lower than the cell pressure until saturation; at this point, it is evolved as a gas at 100% CO_2, as at point 1, the solution was saturated with 15 mol% CO_2. After separating pure CO_2 from the anolyte, the stream is sent through to the cathode compartment (i.e., 2 → 3), where the proton concentration is decreased by the proton ion intercalation reaction. For the sake of charge

Please cite this article in press as: Rahimi et al., Carbon Dioxide Capture Using an Electrochemically Driven Proton Concentration Process, Cell Reports Physical Science (2020), https://doi.org/10.1016/j.xcrp.2020.100033

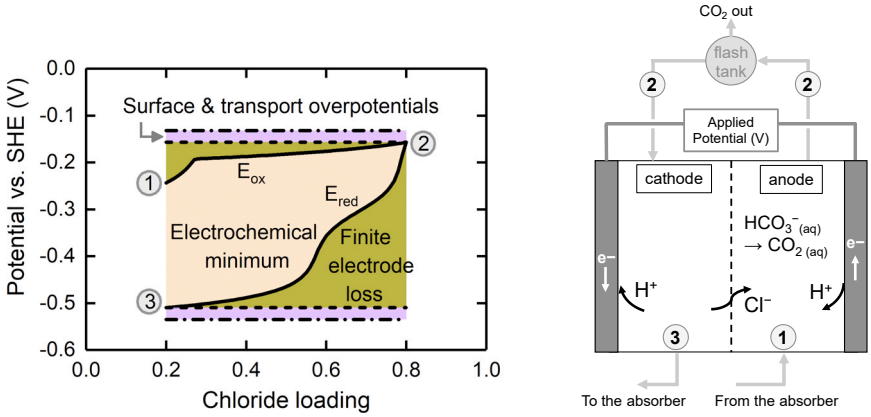

Figure 4. Simulated Potential Distribution as a Function of Chloride Loading along the Length of an Electrochemical Cell

The electrochemical modulation of proton concentration results in a change in x_{Cl} across the cell; therefore, the results were presented as a function of x_{Cl}. In addition to the half-cell equilibrium potentials (i.e., E_{ox} and E_{red}), a finite electrode loss (dashed line) and a surface and transport overpotential (dotted and dashed line) were considered. The highlighted areas between the curves are proportional to specific energetics. The potentials are presented with respect to the SHE. The potentials of the anode and cathode inlets and outlets are labeled in the graph and the schematic. At the anode, deintercalation of proton ions through the oxidation reaction ($XH_{n\,(s)} \rightleftharpoons X_{(s)} + n\,H^+_{(aq)} + n\,e^-$) results in a shift in the equilibrium toward CO_2 formation. The absorbent is regenerated in the cathode chamber where proton ions are intercalated through the reduction reaction ($X_{(s)} + n\,H^+_{(aq)} + n\,e^- \rightleftharpoons XH_{n\,(s)}$).

neutrality, chloride ions are transferred to the anode compartment, resulting in a decrease in chloride loading across the cathode compartment. The potential profile (E_{red}) follows the same trend as a typical diprotic acid titration curve, suggesting that the potential needed to modulate the proton concentration in the cathode compartment is mainly affected by the buffer capacity of the $CO_2/HCO_3^-/CO_3^{2-}$ system. The area between the E_{ox} and E_{red} curves is proportional to the minimum electrochemical work (W_{min}) needed to desorb CO_2. A W_{min} of 22.7 kJe/mol CO_2 was calculated.

In addition to the equilibrium potentials, we considered other overpotential losses, including finite electrode and surface and transport overpotentials. The finite electrode loss, which originates from a uniform distribution of potential on the electrode surface, was calculated to be as high as 13.9 kJe/mol CO_2. This value is significant compared with the minimum electrochemical work (22.7 kJe/mol CO_2). The finite electrode loss due to having a single electrode can be minimized by using segmented electrodes. For example, for 2 and 4 segmented electrode configurations, finite electrode loss could be reduced to 9.93 and 4.9 kJe/mol CO_2, respectively. Figure 5 illustrates how using a segmented electrode configuration minimizes the finite electrode loss, as the highlighted areas corresponding to this loss (i.e., olive areas) are decreased compared to those presented in Figure 4. Additional surface and transport overpotentials of 25 mV were considered to drive the desired current. The energetics corresponding to this overpotential was estimated to be 5.6 kJe/mol CO_2. Therefore, the total electrochemical work required for the proposed capture process with segmented electrodes that could efficiently intercalate/deintercalate protons was estimated to be 33.2 kJe/mol CO_2.

The electrochemical work for the developed proton concentration process was further compared with similar electrochemical-based systems of CO_2 capture (Figure 6). The total energy required for the proton concentration process (33.2 kJe/mol

Please cite this article in press as: Rahimi et al., Carbon Dioxide Capture Using an Electrochemically Driven Proton Concentration Process, Cell Reports Physical Science (2020), https://doi.org/10.1016/j.xcrp.2020.100033

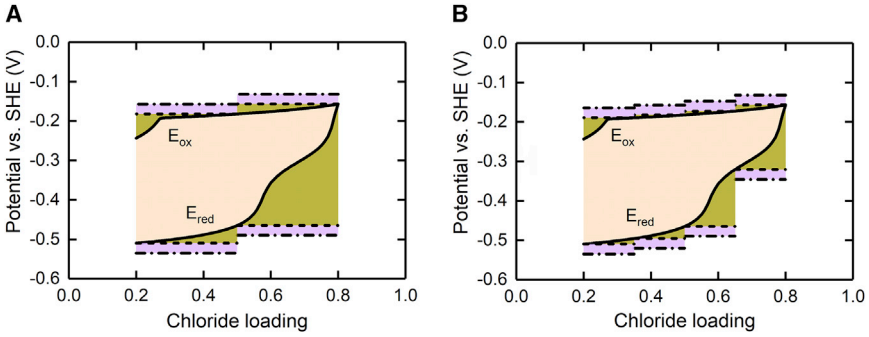

Figure 5. Simulated Potential Distribution for Segmented Electrode Configurations

(A and B) The potentials were estimated as a function of chloride loading along the length of an electrochemical cell with (A) two and (B) four segmented electrodes. The half-cell equilibrium potentials (i.e., E_{ox} and E_{red}), finite electrode losses (dashed line) and surface and transport overpotentials (dotted and dashed line) were considered. The highlighted areas between the curves are proportional to specific energetics, including electrochemical minimum (beige area), finite electrode loss (olive areas), and surface and transport overpotentials (pink areas). The potentials are presented with respect to SHE.

CO_2) was comparable to that of the previously discussed EMAR process (31.3 kJe/mol CO_2).[27] The minimum electrochemical energetics of the proton concentration process (i.e., proportional to the area between E_{ox} and E_{red} curves) was slightly higher than that of the EMAR, mainly because the electrochemical reaction in the EMAR system involves 2 electrons (i.e., $Cu^0 \rightarrow Cu^{2+} + 2e^-$),[24] whereas the reaction considered here is a 1-electron transfer reaction. Although the proton concentration process requires higher electrochemical work to desorb CO_2, it offers some benefits compared with the EMAR system. An amine-based absorbent is used in the EMAR process, which has been shown to have some issues related to corrosion and degradation.[9,34] In the present study, however, we used K_2CO_3, which offers lower cost and toxicity, together with lower rates of corrosion and degradation. In addition, the proton concentration process relies on proton intercalation/deintercalation into and from the electrode, rather than plating or corroding a copper electrode, leading to a potentially more stable reversible system. It is worth noting that efforts are continuing on many aspects of the EMAR system to scale it up and implement it in an actual power plant.

The developed proton concentration process required less energy than the similar MCDI system operated with different applied current densities. For example, the total energetics of the proton concentration process was up to 30% less than that of an MCDI that aimed to separate CO_2 from a stream containing 15 mol% CO_2.[25] In the MCDI system, two types of energy losses are introduced: ohmic loss, due to ohmic resistance, and non-ohmic loss, such as concentration polarization.[25] At the higher current density used in the MCDI work (e.g., 0.6 A m^{-2}), it was found that a major part of the energetics (up to 70%) was due to ohmic loss. Reducing ohmic loss (ohmic resistance) could be done by reducing the electrode distance or using a background electrolyte salt, both of which are challenging to implement in the MCDI system. The electrodes are already very close to each other (~250 μm) and decreasing that distance further may cause an electrical shortage in the circuit. Using a background electrolyte to reduce ohmic resistance is also not feasible because the membranes that cover the electrodes are selective only to the charge of the ion; transfer of the background ions rather than proton and bicarbonate ions through the membranes results in a decreased Faradaic efficiency. In contrast, the energetics of our proposed proton concentration process could be decreased by optimizing the

Cell Reports
Physical Science

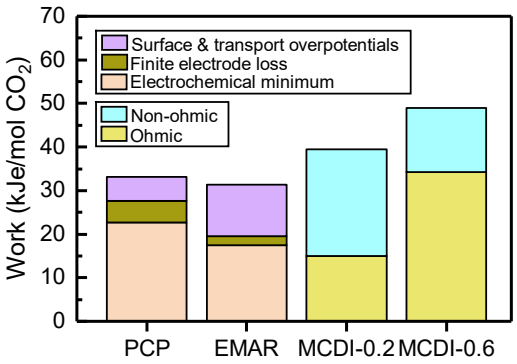

Figure 6. Comparison of the Electrochemical Energetics of the Developed Proton Concentration Process with Other Electrochemical-Based CO_2 Capture Systems

The electrochemical energetics calculated in this study were compared with those of an electrochemically mediated amine regeneration (EMAR) process operated at 1 bar and isothermally at 50°C,[27] and a membrane capacitive deionization (MCDI) operated at current densities of 0.2 A m^{-2} (MCDI-0.2) and 0.6 A m^{-2} (MCDI-0.6).[25] The electrochemical work was estimated to separate CO_2 gas from a stream containing 15 mol% CO_2 and 85 mol% N_2.

background electrolyte or by using an electrode with a higher number of electrons transferred in the electrochemical reaction (i.e., a higher *n*).

Electrode Development

Based on the thermodynamic model developed above, we showed that CO_2 could be desorbed efficiently from a K_2CO_3 solution by electrochemically modulating the proton concentration (i.e., solution pH). Proton intercalation/deintercalation into and from an electrode matrix was considered the main Faradaic reaction. Here, an MnO_2-based electrode, previously shown to be a good proton host,[31,33,35] was developed.

MnO_2 Electrode Characterization

The MnO_2 electrodes were characterized by X-ray photoelectron spectroscopy (XPS) to analyze their chemical state. The XPS survey spectrum showed several peaks related to Mn and O, including Mn 2p and O 1s core-level spectra (Figure S1). The Mn 2p core-level spectrum displayed 2 peaks at binding energies of 653.9 and 642.3 eV, corresponding to the spin-orbit doublet of Mn $2p_{1/2}$ and Mn $2p_{3/2}$, respectively (Figure 7A). The spin-energy separation of 11.6 eV confirmed the formation of MnO_2, which is consistent with observations for similar materials.[33,36] In addition, the binding energy obtained for Mn $2p_{3/2}$ (642.3 eV) was in good agreement with that corresponding to the Mn(IV) oxidation state (642.6 eV),[37] further confirming the formation of MnO_2. Because of the importance of O in the MnO_2 matrix, the O 1s core-level spectrum was studied (Figure 7B). The O 1s spectrum could be deconvoluted into 2 main constituent peaks corresponding to different O-containing species. The peaks were related to the Mn–O–Mn bond (529.7 eV) for the tetravalent oxide and the Mn–OH bond (531.8 eV) for a hydrated trivalent oxide.[33] Based on the areas under these peaks and the procedure previously developed,[33] the atomic ratio of Mn:O was calculated to be 1:1.93. Therefore, based on the results from the XPS analysis, it can be concluded that MnO_2 was formed successfully.

Cyclic voltammetry (CV) was used to study the capacitance behavior of the fabricated electrodes (Figure 8). The MnO_2-based electrodes showed a mainly rectangular CV curve, characteristic of a pseudocapacitance material.[33] This is in good agreement with the previously reported results for MnO_2 electrodes, which confirmed that the charge storage mechanism was a Faradaic reaction together with intercalation (i.e., a

Cell Reports
Physical Science

CellPress

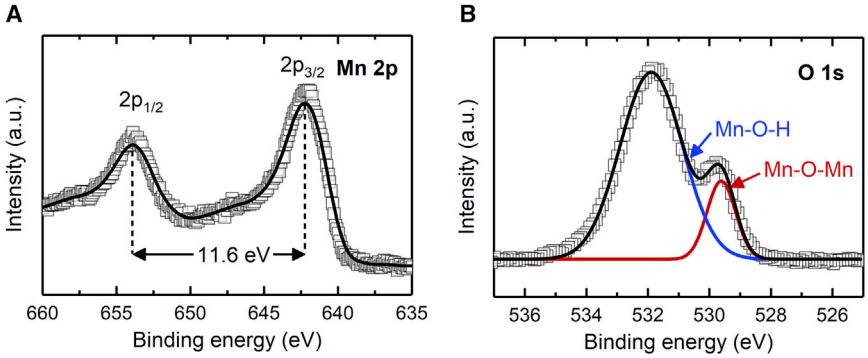

Figure 7. XPS Analysis of the Fabricated Electrode

(A and B) Mn 2p (A) and O 1 s (B) core-level spectra for the fabricated MnO_2 electrodes. The red and blue lines in the O 1s spectrum correspond to the Mn–O–Mn and Mn–OH bonds, respectively.

pseudocapacitance behavior).[38] The capacitance was normalized by the mass of the active material (known as specific capacitance), enabling relevant comparisons between MnO_2 materials fabricated with a casting technique. Using CV, the specific capacitances of the MnO_2 electrodes with carbon felt and carbon cloth substrates were calculated to be 85 and 144 F g^{-1}, respectively (Figure 8A). These values matched those previously reported (ranging from 50 to 220 F g^{-1}).[33,39–41] MnO_2-based electrodes with higher capacitances can be obtained through more advanced fabrication methods such as electrodeposition and atomic layer deposition, which will be investigated in the future development of proton concentration process (PCPs).

Despite a lower specific capacitance, the MnO_2 electrode with carbon felt substrate had a higher geometrical capacitance (201 mF cm^{-2} for carbon felt, 110 mF cm^{-2} for carbon cloth; Figure 8B). This finding could be related to the amount of MnO_2 material cast onto the substrate and its accessibility for electrochemical reactions. Compared with the carbon cloth, the carbon felt substrate provides a higher active surface area for the same geometrical area. This is mainly due to larger spaces between the fibers in carbon felt, which allow MnO_2 material to be cast not only onto the surface but also throughout the substrate. This was also confirmed by the experimental measurement in which the weight of the substrate was measured before and after the casting. The mass loading of the MnO_2 material on the carbon felt substrate was 15 mg cm^{-2}, whereas it was 4 mg cm^{-2} for the carbon cloth. Figure 9 illustrates the difference between the surface properties of the carbon cloth and carbon felt substrates. By inserting MnO_2 materials, capacitance is improved because of the increased surface area of the active material. Adding more material results in the formation of a thick layer (compared with the thin film that normally forms at low MnO_2 loadings). The MnO_2 sites of lower layers in a thick electrode are not necessarily accessible to the electrochemical reaction,[33] resulting in a lower specific capacitance of carbon felt electrodes. Compared with specific capacitance, geometrical capacitance has better practical meaning because the concept developed here relies on electrode geometric areas to provide sufficient hosts for proton intercalation/deintercalation reactions.

The carbon-based materials used as electrode substrates could also store charge; however, their contribution was much smaller than that of the MnO_2 material, as reflected by the significantly higher current generated in the CV analysis for the electrode with MnO_2. This is mainly because the MnO_2 materials store charge as a pseudocapacitance, whereas carbon materials rely on the electrical double-layer

Please cite this article in press as: Rahimi et al., Carbon Dioxide Capture Using an Electrochemically Driven Proton Concentration Process, Cell Reports Physical Science (2020), https://doi.org/10.1016/j.xcrp.2020.100033

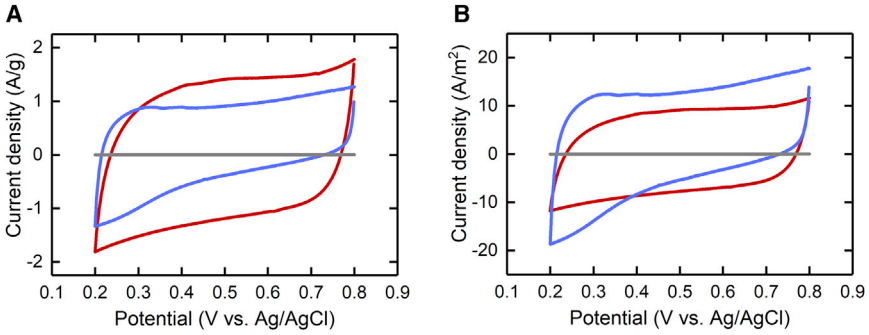

Figure 8. Cyclic Voltammetry of the Fabricated Electrode

(A and B) Cyclic voltammograms were normalized by (A) the mass of active material (specific capacitance) and (B) the area of the electrode (geometrical capacitance) of a pristine carbon cloth (gray line) as well as MnO_2 electrodes cast on carbon cloth (red line) or carbon felt (blue line) substrates. The tests were conducted in a potential range between 0.2 and 0.8 V (versus Ag/AgCl) at a scan rate of 2 mV s^{-1} and using 0.5 M Na_2SO_4 as the electrolyte.

capacitance (the capacity of which is significantly lower than that of a pseudocapacitance).

Modulation of Proton Concentration by MnO_2 Electrodes

A symmetrical electrochemical cell with two MnO_2 electrodes was used to study the rate and reversibility of the proton intercalation/deintercalation reactions. A constant voltage was applied, and current density and solution pH were monitored as two responses. In an ideal system, the current is effectively translated into proton intercalation/deintercalation reactions that, for a solution with a low buffer capacity, can be observed as a change in the solution pH. We tested fabricated MnO_2 electrodes with carbon felt and carbon cloth substrates. The results showed a high rate of proton intercalation/deintercalation reactions with a pH swing ranging from 1.2 to 3 units (Figure 10). The generated current and pH change over >10 cycles were very reversible. We investigated reversibility further under different experimental and operational conditions, and the results showed a significant pH swing that enables the system to effectively capture and release CO_2.

We studied the effect of carbon substrate on the generated current and pH change. The MnO_2 electrodes with carbon felt substrate obtained a higher current, and hence, a higher pH swing (3 and 1.2 units of pH swing for carbon felt and carbon cloth, respectively; Figure 10). The higher current and pH swing of the carbon felt-based MnO_2 electrode can be attributed to the higher geometrical capacitance of carbon felt compared with carbon cloth, as shown in the CV measurements (Figure 8B). Although using carbon felt-based electrodes offers higher current and pH swing, this substrate causes a greater pressure drop along the cell when integrated into a flow cell, mainly because of its large pore size and relatively larger thickness. Therefore, the use of carbon felt as the MnO_2 electrode substrate for a flow-based CO_2 capture system should be carefully investigated in the future to avoid significant pressure drops and extra energy consumption.

These experiments were designed to study the rate and reversibility of the electrode for proton intercalation/deintercalation reactions using a low-buffer capacity solution (i.e., KCl) in which the proton concentration change can be effectively translated into the solution pH change. For future developments in which these electrodes are used in a PCP to desorb CO_2, the experiments must be done with an electrolyte containing both K_2CO_3 and KCl.

Please cite this article in press as: Rahimi et al., Carbon Dioxide Capture Using an Electrochemically Driven Proton Concentration Process, Cell Reports Physical Science (2020), https://doi.org/10.1016/j.xcrp.2020.100033

Cell Reports
Physical Science

CellPress

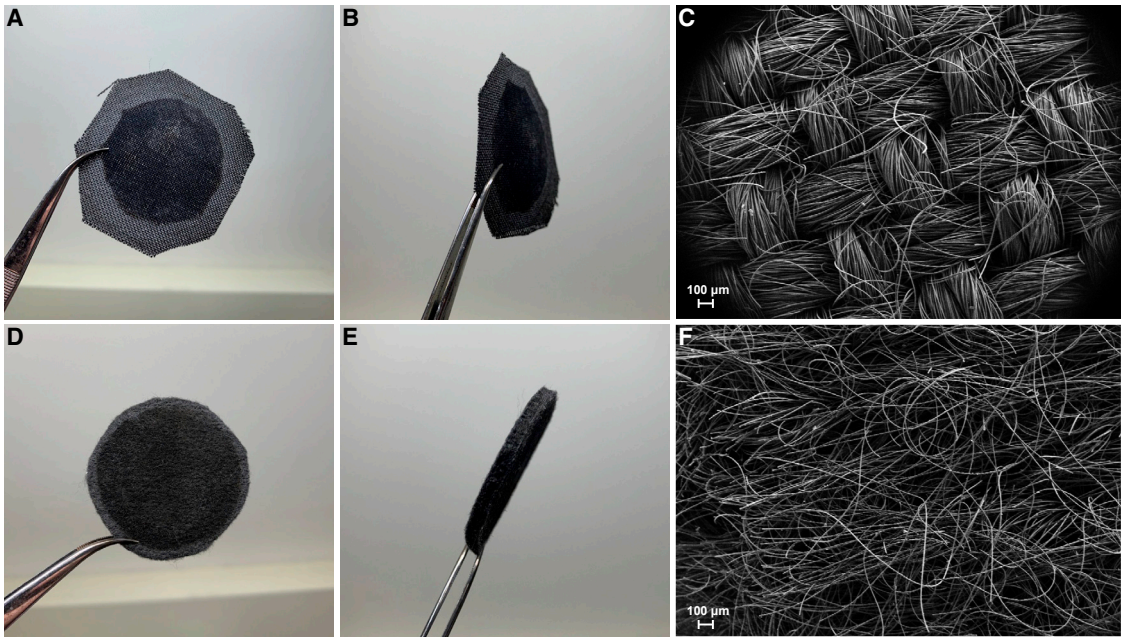

Figure 9. An Illustration of the Difference between Carbon Cloth and Carbon Felt Substrates

(A–F) The thickness of carbon cloth (A and B) and carbon felt (D and E) were measured to be 0.35 and 3 mm, respectively. The SEM images exhibit the difference between the string formation of the carbon cloth (C) and carbon felt (F). For both substrates, MnO_2 materials were cast onto the same geometrical area of 7.1 cm^2.

DISCUSSION

We introduced a new approach based on a proton concentration electrochemical cell for CO_2 capture using MnO_2, which was shown to be a good proton intercalating material, as the electrode. The developed activity-based thermodynamic model was able to predict speciation, which was later validated by experimental measurements under different conditions. The model was also able to estimate the potential profile to be applied to the electrochemical cell for CO_2 desorption. The electrochemical work requirement for the proposed proton concentration process was estimated to be 33.2 kJe/mol CO_2, which is comparable to that of the EMAR process (31.3 kJe/mol CO_2) and ~30% lower than that of the MCDI capture system (49 kJe/mol CO_2) operating at a reasonable current density. The electrochemical energy consumption of the proposed approach could be lowered by using electrodes with a higher number of electrons transfer (i.e., a higher *n*), by process optimization, and by identifying new chemistries. In addition to the electrochemical work, other process-based energetics related to compressors and pumps should be considered in future studies to be able to meaningfully compare this technology with conventional methods of CO_2 capture (e.g., thermal processes).

The proposed proton concentration process is in the early stage of development, and several modifications must be considered in terms of cell design and configuration and process operation. Here, CO_2 desorption and solution pH swing processes were studied independently in two sets of controlled experiments. In one set, we showed that CO_2 could be desorbed linearly by introducing proton ions, despite the high buffering capacity of the absorbent at high CO_2 loadings. We did these experiments by adding HCl to mimic the proton concentration change modulated by an electrochemical cell. In another set of experiments, we showed experimentally that the solution pH could be effectively modulated through reversible cycles by

Please cite this article in press as: Rahimi et al., Carbon Dioxide Capture Using an Electrochemically Driven Proton Concentration Process, Cell Reports Physical Science (2020), https://doi.org/10.1016/j.xcrp.2020.100033

Cell Reports
Physical Science

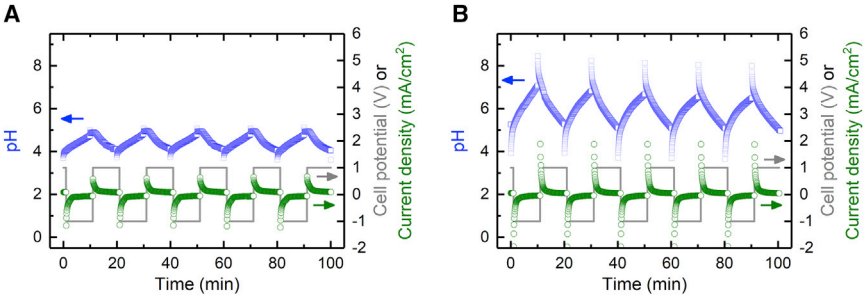

Figure 10. Modulation of Proton Concentration by MnO_2 Electrodes

(A and B) Current density (green symbols) and solution pH (blue symbols) of a symmetrical cell with MnO_2 electrodes cast onto (A) carbon cloth and (B) carbon felt substrates were recorded. A constant potential of 1 V was applied, and the polarity was changed at intervals of 10 min for 10 cycles (gray line). A solution of 0.5 M KCl, which has a low buffer capacity, was used as the electrolyte.

applying constant potential across a symmetrical cell with two MnO_2 electrodes. In applications, the insights from these two sets of experiments must be combined to design and operate a system in which CO_2 is desorbed from the anode compartment of an electrochemical cell where the deintercalation of proton shifts the CO_2 hydration equilibrium toward gas release. In addition, to implement the proposed proton concentration approach in practice, a continuous process of CO_2 capture and release by integrating a K_2CO_3-based absorber and an MnO_2-based electrochemical cell is being developed and will be reported in a future communication.

EXPERIMENTAL PROCEDURES

Thermodynamic Modeling

A comprehensive thermodynamic model was developed to determine the equilibrium speciation in the absorber and desorber, predict the electrochemical behavior, and, finally, estimate the energy requirement to electrochemically modulate the proton concentration for CO_2 desorption. To be able to desorb CO_2, the absorbent capture mechanism should be based on the hydration of CO_2 rather than the carbamate formation. Therefore, K_2CO_3, in which CO_2 is absorbed as bicarbonate (HCO_3^-) and carbonate (CO_3^{2-}) (Equations 1 and 2), was selected as the absorbent in this study. K_2CO_3 is widely used in thermal scrubbing carbon capture processes because of its several advantages, including low degradation rate, ease of regeneration, low cost, and high CO_2 absorption capacity.[7]

Model Development for the Absorption and Desorption Processes

The model developed for the equilibrium speciation was adapted from a similar model we introduced for another electrochemically based CO_2 capture system using amines.[27] K_2CO_3 as the absorbent and KCl as the background electrolyte are used in the present article; hence, the reaction system of CO_2–K–Cl–H_2O was considered in the model. All of the relevant equilibrium speciation reactions were taken into account, with the equilibrium constants tabulated in Table S1. Specifically, we developed an activity-based model that offers more accurate estimates of solution equilibria than those of the concentration-based systems, especially for systems with high ionic strength such as PCP. This is also important for estimating the electrochemical parameters such as potential, since the Nernst equation, the core relation between the pH and potential, uses the activities of the different species. The activities *a* of the various aqueous species *i* are given by:

$$a_i = \gamma_i C_i \quad (4)$$

Please cite this article in press as: Rahimi et al., Carbon Dioxide Capture Using an Electrochemically Driven Proton Concentration Process, Cell Reports Physical Science (2020), https://doi.org/10.1016/j.xcrp.2020.100033

where γ_i is the activity coefficient and C_i is the concentration. The extended Debye-Hückel equation with the B-dot parameter was used to calculate the activity coefficient of the charged species[42]:

$$\log \gamma_i = -\frac{A_{\gamma,10} z_i^2 \sqrt{\bar{I}}}{1 + \alpha_i B_\gamma \sqrt{\bar{I}}} + \dot{B}\bar{I} \quad (5)$$

where $A_{\gamma,10}$ and B_γ are the Debye-Hückel parameters, z is the electrical charge of the species, α is the hard core diameter of the species, $\dot{B}$ is the characteristic B-dot parameter, and $\bar{I}$ is the ionic strength of the solution. The activity coefficients for all of the neutral species, except $CO_{2\ (aq)}$ and H_2O, were set to unity. The activity coefficients for $CO_{2\ (aq)}$ and H_2O are described in Data S2. A more detailed description of the activity coefficient model and the speciation calculations can be found in our previous study.[27] The developed activity-based model and the mass and charge balance equations (Data S1) were used to calculate all of the speciations, including CO_2 (to evaluate the CO_2 loading) and proton (to evaluate the solution pH) in the absorber and the desorber.

Model Development for the Electrochemical Cell

To describe the electrochemical behavior of the system, an electrochemical thermodynamic cycle was constructed. The Faradaic intercalation/deintercalation of protons during the reduction-oxidation reaction results in a proton concentration gradient across the length of the cell. For the sake of electrical neutrality and electrical circuit completion, migration of Cl^- ions (present as the background electrolyte) through the anion-exchange membrane from the cathode to the anode compartment was assumed. To better represent the results, the Cl^- concentration (C_{Cl}) in each compartment was normalized by the initial absorbent concentration (C_{abs}) and defined as the chloride loading, x_{Cl} ($x_{Cl} = C_{Cl}/C_{abs}$). To construct the electrochemical thermodynamic cycle, the half-cell equilibrium potential at any chloride loading was calculated according to the Nernst equation[43]:

$$E = E_0 + \frac{RT}{nF} \ln \alpha_{H^+} \quad (6)$$

where E_0 is the standard electrode potential for the intercalation reaction (i.e., $X + n\ H^+ + n\ e^- \rightarrow XH_n$; n, the number of electrons transferred), R is the gas constant (8.314 J mol^{-1} K^{-1}), T is the absolute temperature (K), F is the Faraday constant (96485 C mol^{-1}), and α_{H^+} is the activity of proton ions.

Faradaic reduction and oxidation reactions of the electrode result in the generation of an electric current. The generated current affects the solution pH by introducing H^+ ions into the anolyte and withdrawing ions from the catholyte, resulting in a change in the chloride loading across the cell. Therefore, the current generated due to a small change in chloride loading dx_{Cl} could be described as:

$$dI = \frac{nFQx_w}{\eta_{int}} dx_{Cl} \quad (7)$$

where Q is the mass flow rate of the solution through the compartment, x_w is the mass fraction of water, and η_{int} is the intercalation efficiency. Intercalation efficiency can be defined as the number of moles of proton intercalated per mole of electron transferred. For an ideal electrode, all of the electrical current is consumed by the proton intercalation, resulting in an intercalation efficiency of unity.

By calculating the potential (Equation 6) and the current (Equation 7) as a function of the solution pH and chloride loading, the minimum electrochemical work (W_{min}; in

Please cite this article in press as: Rahimi et al., Carbon Dioxide Capture Using an Electrochemically Driven Proton Concentration Process, Cell Reports Physical Science (2020), https://doi.org/10.1016/j.xcrp.2020.100033

kJe/mol CO_2) needed to drive the reactions and desorb CO_2 was estimated as follows:

$$W_{min} = \frac{1}{F_{m.CO2}} \left(\int_{x_{Cl}} E_{ox}\, dl - \int_{x_{Cl}} E_{red}\, dl \right) \quad (8)$$

where $F_{m,CO2}$ is the molar rate of CO_2 captured, and E_{ox} and E_{red} are the oxidation and reduction equilibrium potentials, respectively. In practice, an electrochemical cell cannot be operated at its equilibrium potential. In addition to the equilibrium potentials (E_{ox} and E_{red}), several overpotential terms contribute to the total work needed by the electrochemical cell. For example, the overpotential loss due to having a single electrode, which inherently develops the same potential at any position along the electrode, should be considered. This overpotential loss was previously introduced as a finite electrode loss, and the use of segmented electrodes, in which different electrode segments were maintained at different cell voltages, was proposed to minimize it.[27] In addition to the finite electrode loss, additional surface and transport-related overpotentials need to be supplied to drive the desired current density and achieve the desired shift in chloride loading. For this study, we considered a surface and transport overpotential of 25 mV. Similar to W_{min}, the electrochemical work associated with these overpotentials could be calculated using Equation 8 with appropriate potential values.

Solution Preparation for Absorption and Desorption Experiments

To verify the model developed for the absorption process, a solution of K_2CO_3 (Sigma-Aldrich; 0.5 or 1 mol kg^{-1}) was purged with various concentrations of CO_2 mixed with N_2 (15 mol% or 100% CO_2) at a constant temperature of 23°C or 50°C. Pure CO_2 and N_2 gases (Airgas) were mixed at different flow rates using 2 mass flow controllers (00284UI, Cole Parmer) to obtain different gas compositions. The solutions were purged in a 250-mL stirred 3-neck flask equipped with a gas dip tube, a reflux condenser, and a temperature probe (set to either 23°C or 50°C). The CO_2 loading (x_{CO2}; defined as $x_{CO2} = C_{CO2}/C_{K+}$) and solution pH were measured after purging for each absorption experiment. The desorption experiment was conducted by adding certain concentrations of HCl (37%, Sigma-Aldrich; 0.2, 0.4, 0.6, 0.8, and 1 mol kg^{-1}) into 0.5 mol kg^{-1} K_2CO_3 saturated with 15 mol% CO_2 and 85 mol% N_2 at 50°C. The CO_2 loading and solution pH were recorded at each added HCl concentration. To more accurately compare the simulated equilibrium conditions and the experimental values, the solutions were purged overnight to reach equilibrium, owing to the low absorption kinetics of K_2CO_3 for CO_2 capture (Figure S2). For future practical implementations of PCP for CO_2 capture, strategies to improve the absorption kinetics such as the use of a rate promoter must be considered.

CO_2 Capacity and pH Measurements

The CO_2 loading for each experiment was estimated by measuring the volume of gaseous CO_2 released upon acidification of the sample. A sample of 1 mL solution was mixed with 1 mL 4 M HCl in a closed gas-tight glass vial. The gas evolved was sent to a U-tube manometer to measure the increase in gas pressure and calculate the CO_2 loading present in the solution (Figure S3). The solution pH was measured using a pH probe (Orion PerpHecT ROSS) calibrated at 23°C and 50°C before the experiment.

Electrode Fabrication

The MnO_2 powder was synthesized by following a previously reported coprecipitation method in which $KMnO_4$ (Alfa Aesar) and $MnSO_4$ (Alfa Aesar) were mixed at

Please cite this article in press as: Rahimi et al., Carbon Dioxide Capture Using an Electrochemically Driven Proton Concentration Process, Cell Reports Physical Science (2020), https://doi.org/10.1016/j.xcrp.2020.100033

room temperature in a 2:3 molar ratio, leading to a dark brown precipitate according to[32,39,44]:

$$2KMnO_4 + 3MnSO_4 + H_2O \rightarrow 5MnO_2\downarrow + K_2SO_4 + 2\,H_2SO_4 \quad (9)$$

The formed MnO_2 precipitates were washed several times, collected by centrifugation, and dried overnight in a vacuum oven at 70°C. The synthesized MnO_2 was mixed with carbon black (Ketjenblack EC-600JD) and polyvinylidene fluoride (Sigma-Aldrich; average molecular weight ~180,000) in a 7:2:1 weight ratio to form a composite. Then, 1-methyl-2-pyrrolidinone (Sigma-Aldrich; 2 mL 0.1 g^{-1} MnO_2) was added to the composite while it was being homogeneously mixed, and the resulting slurry was cast onto 2 different carbon-based substrates, carbon cloth and carbon felt, using a leveled glass plate. Commercially available carbon cloth and carbon felt (AvCarb Material Solutions) were treated to improve surface hydrophilicity by soaking overnight in a mixed solution of concentrated sulfuric and nitric acids (3:1 v:v) at room temperature.[45] After applying the composite to the carbon substrates, the electrodes were dried overnight in a vacuum oven at 70°C. An illustration of the electrode fabrication using the coprecipitation method can be found in Figure S4 and in the literature.[32]

Electrode Characterization

The fabricated electrodes were characterized using XPS to evaluate their chemical states. The XPS analysis was obtained on a Thermo Scientific K-Alpha+ XPS equipped with Al (Kα) source with a spot size of 400 μm. The binding energies were calibrated with respect to the C_{1s} peak at 284.5 eV. Survey spectra were collected with a step size of 1 eV and an accumulation of 2 scans. High-resolution spectra were collected with a step size of 0.1 eV and an accumulation of 10 scans. The microstructure of the carbon substrates was observed with a Zeiss Merlin high-resolution scanning electron microscope (SEM).

Capacitance Measurement

The CV technique was used to study the capacitance properties of the MnO_2 electrodes. The CV was performed in a 3-electrode configuration using a Ag/AgCl (+0.211 V versus standard hydrogen electrode [SHE]; RE-5B; BASi) reference electrode and a platinum wire as counter electrode. As the working electrode, a circular MnO_2 electrode (3 mm diameter) was attached to the glassy carbon electrode (3 mm diameter; BASi) using conductive carbon tape (Ted Pella, 16084-4, 3 mm). To be consistent with similar studies on MnO_2 electrodes, CVs were run over the potential range of 0.2–0.8 V with a scan rate of 2 mV s^{-1} and using 0.5 M Na_2SO_4 as the electrolyte. The capacitance was normalized by either the mass of active material (i.e., specific capacitance) or the geometrical surface of the electrode (i.e., geometrical capacitance). The normalized capacitance, C_n (in F g^{-1} or F cm^{-2}), was calculated as[29]:

$$C_n = \frac{\int_{V_1}^{V_2} I\,dV}{2\,\chi\,\nu\,\Delta V} \quad (10)$$

where I is the current (A), χ is the mass of active material (g) or the geometric area of the electrode (cm^2), ν is the scan rate in CV tests (V s^{-1}), V_1 and V_2 are vertex potentials (0.2 and 0.8 V, respectively), and ΔV is the potential window (0.6 V).

Electrochemical Cell Configuration and Operation

A batch-type symmetrical electrochemical cell with two MnO_2 electrodes was used to investigate the rate and reversibility of the proton intercalation/deintercalation reaction. The cell used for the tests was constructed as previously

Cell Reports
Physical Science

CellPress

described.[46,47] Briefly, it consisted of cathode and anode chambers, each 2 cm long and 3 cm diameter, separated by an anion-exchange membrane (Selemion AMV, Asashi Glass). Two identical MnO_2 electrodes with diameters of 3 cm (geometrical area of 7.1 cm^2) were used as the electrodes, which were placed at the end of each chamber. To uniformly distribute the potential over the electrode surface and collect the generated current, 2 pieces of stainless steel (100 × 100 mesh; McMaster-Carr) with the same diameters of 3 cm were inserted behind the electrodes and attached using conductive carbon tape. The solution pH of the anolyte, where CO_2 is desorbed, was monitored using a pH probe. To facilitate the mass transfer of ions to the electrode, the anolyte was mixed using a magnetic stirrer. The cell was operated at a constant voltage (E) of 1 V and the polarity was changed (i.e., $E = -1$ V) every 10 min using a potentiostat (PARSTAT PMC-1000, Princeton Applied Research). While the potential was applied, the anolyte pH and generated current density (normalized to the geometrical area of the electrode) were recorded. A solution of 0.5 mol kg^{-1} KCl (Sigma-Aldrich) was used as the electrolyte. This solution exhibits a low buffer capacity; thus, the change in solution pH can be easily correlated with the rate of the proton intercalation/deintercalation reaction.

Data and Code Availability

All of the data associated with the studies are represented in the manuscript and supplemental information. The raw data are available from the Lead Contact upon reasonable request.

SUPPLEMENTAL INFORMATION

Supplemental Information can be found online at https://doi.org/10.1016/j.xcrp.2020.100033.

ACKNOWLEDGMENTS

The authors would like to thank Dr. Katherine Phillips, Department of Chemical Engineering at Massachusetts Institute of Technology (MIT), for running the XPS tests. We also acknowledge Dr. David Calabro from the Corporate Strategic Research Laboratory of ExxonMobil Research and Engineering for useful discussions. The research was supported by ExxonMobil.

AUTHOR CONTRIBUTIONS

Conceptualization, M.R.; Methodology, M.R. and G.C.; Software, S.H. and M.W.; Validation, M.R. and G.C.; Investigation, M.R. and G.C.; Writing – Original Draft, M.R.; Writing – Review & Editing, M.R., G.C., M.W., and T.A.H.; Visualization, M.R., G.C., and T.A.H.; Supervision, T.A.H. and M.P.

DECLARATION OF INTERESTS

The authors declare no competing interests.

Received: October 4, 2019
Revised: December 23, 2019
Accepted: February 11, 2020
Published: March 18, 2020

REFERENCES

1. Hashimoto, K. (2019). Global Temperature and Atmospheric Carbon Dioxide Concentration. In Global Carbon Dioxide Recycling for Global Sustainable Development by Renewable Energy, K. Hashimoto, ed. (Springer), pp. 5–17.
2. Benson, S.M., and Orr, F.M. (2008). Carbon dioxide capture and storage. MRS Bull. *33*, 303–305.
3. Leung, D.Y., Caramanna, G., and Maroto-Valer, M.M. (2014). An overview of current status of carbon dioxide capture and storage technologies. Renew. Sustain. Energy Rev. *39*, 426–443.
4. Rheinhardt, J.H., Singh, P., Tarakeshwar, P., and Buttry, D.A. (2017). Electrochemical capture and release of carbon dioxide. ACS Energy Lett. *2*, 454–461.
5. Bui, M., Adjiman, C.S., Bardow, A., Anthony, E.J., Boston, A., Brown, S., Fennell, P.S., Fuss, S., Galindo, A., and Hackett, L.A. (2018). Carbon capture and storage (CCS): the way forward. Energy Environ. Sci. *11*, 1062–1176.
6. Rochelle, G.T. (2009). Amine scrubbing for CO2 capture. Science *325*, 1652–1654.
7. Borhani, T.N.G., Azarpour, A., Akbari, V., Alwi, S.R.W., and Manan, Z.A. (2015). CO2 capture with potassium carbonate solutions: a state-of-the-art review. Int. J. Greenh. Gas Control *41*, 142–162.
8. Rochelle, G.T. (2012). Thermal degradation of amines for CO2 capture. Curr. Opin. Chem. Eng. *1*, 183–190.
9. Gouedard, C., Picq, D., Launay, F., and Carrette, P.-L. (2012). Amine degradation in CO2 capture. I. A review. Int. J. Greenh. Gas Control *10*, 244–270.
10. Dutcher, B., Fan, M., and Russell, A.G. (2015). Amine-based CO2 capture technology development from the beginning of 2013-a review. ACS Appl. Mater. Interfaces *7*, 2137–2148.
11. Dumée, L., Scholes, C., Stevens, G., and Kentish, S. (2012). Purification of aqueous amine solvents used in post combustion CO2 capture: a review. Int. J. Greenh. Gas Control *10*, 443–455.
12. Porter, R.T., Fairweather, M., Kolster, C., Mac Dowell, N., Shah, N., and Woolley, R.M. (2017). Cost and performance of some carbon capture technology options for producing different quality CO2 product streams. Int. J. Greenh. Gas Control *57*, 185–195.
13. Mumford, K.A., Smith, K.H., Anderson, C.J., Shen, S., Tao, W., Suryaputradinata, Y.A., Qader, A., Hooper, B., Innocenzi, R.A., and Kentish, S.E. (2011). Post-combustion capture of CO2: results from the solvent absorption capture plant at Hazelwood power station using potassium carbonate solvent. Energy Fuels *26*, 138–146.
14. Bhosale, R.R., Kumar, A., AlMomani, F., Ghosh, U., AlNouss, A., Scheffe, J., and Gupta, R.B. (2016). CO2 capture using aqueous potassium carbonate promoted by ethylaminoethanol: a kinetic study. Ind. Eng. Chem. Res. *55*, 5238–5246.
15. Grimekis, D., Giannoulidis, S., Manou, K., Panopoulos, K.D., and Karellas, S. (2019). Experimental investigation of CO2 solubility and its absorption rate into promoted aqueous potassium carbonate solutions at elevated temperatures. Int. J. Greenh. Gas Control *81*, 83–92.
16. Thee, H., Nicholas, N.J., Smith, K.H., da Silva, G., Kentish, S.E., and Stevens, G.W. (2014). A kinetic study of CO2 capture with potassium carbonate solutions promoted with various amino acids: glycine, sarcosine and proline. Int. J. Greenh. Gas Control *20*, 212–222.
17. Huebscher, R., and Babinsky, A.D. (1969). Electrochemical Concentration and Separation of Carbon Dioxide For Advanced Life Support Systems—Carbonation Cell System. SAE Trans. *78*, 2164–2170.
18. Gurkan, B., Simeon, F., and Hatton, T.A. (2015). Quinone reduction in ionic liquids for electrochemical CO2 separation. ACS Sustain. Chem. Eng. *3*, 1394–1405.
19. Scovazzo, P., Poshusta, J., DuBois, D., Koval, C., and Noble, R. (2003). Electrochemical separation and concentration of < 1% carbon dioxide from nitrogen. J. Electrochem. Soc. *150*, D91–D98.
20. Apaydin, D.H., Głowacki, E.D., Portenkirchner, E., and Sariciftci, N.S. (2014). Direct electrochemical capture and release of carbon dioxide using an industrial organic pigment: quinacridone. Angew. Chem. Int. Ed. Engl. *53*, 6819–6822.
21. Voskian, S., and Hatton, T.A. (2019). Faradaic electro-swing reactive adsorption for CO 2 capture. Energy Environ. Sci. *12*, 3530–3547.
22. Eisaman, M.D., Alvarado, L., Larner, D., Wang, P., Garg, B., and Littau, K.A. (2011). CO 2 separation using bipolar membrane electrodialysis. Energy Environ. Sci. *4*, 1319–1328.
23. Watkins, J.D., Siefert, N.S., Zhou, X., Myers, C.R., Kitchin, J.R., Hopkinson, D.P., and Nulwala, H.B. (2015). Redox-mediated separation of carbon dioxide from flue gas. Energy Fuels *29*, 7508–7515.
24. Stern, M.C., Simeon, F., Herzog, H., and Hatton, T.A. (2013). Post-combustion carbon dioxide capture using electrochemically mediated amine regeneration. Energy Environ. Sci. *6*, 2505–2517.
25. Legrand, L., Schaetzle, O., de Kler, R.C.F., and Hamelers, H.V.M. (2018). Solvent-Free CO_2 Capture Using Membrane Capacitive Deionization. Environ. Sci. Technol. *52*, 9478–9485.
26. Stern, M.C., and Hatton, T.A. (2014). Bench-scale demonstration of CO2 capture with electrochemically-mediated amine regeneration. RSC Advances *4*, 5906–5914.
27. Wang, M., Hariharan, S., Shaw, R.A., and Hatton, T.A. (2019). Energetics of electrochemically mediated amine regeneration process for flue gas CO2 capture. Int. J. Greenh. Gas Control *82*, 48–58.
28. Wang, M., Rahimi, M., Kumar, A., Hariharan, S., Choi, W., and Hatton, T.A. (2019). Flue gas CO2 capture via electrochemically mediated amine regeneration: system design and performance. Appl. Energy *255*, 113879.
29. Shi, W., Zhou, X., Li, J., Meshot, E.R., Taylor, A.D., Hu, S., Kim, J.-H., Elimelech, M., and Plata, D.L. (2018). High-performance capacitive deionization via manganese oxide-coated, vertically aligned carbon nanotubes. Environ. Sci. Technol. Lett. *5*, 692–700.
30. Wang, X., Myers, B.D., Yan, J., Shekhawat, G., Dravid, V., and Lee, P.S. (2013). Manganese oxide micro-supercapacitors with ultra-high areal capacitance. Nanoscale *5*, 4119–4122.
31. Kuo, S.-L., and Wu, N.-L. (2006). Investigation of pseudocapacitive charge-storage reaction of MnO2• nH2O supercapacitors in aqueous electrolytes. J. Electrochem. Soc. *153*, A1317–A1324.
32. Kim, T., Logan, B.E., and Gorski, C.A. (2017). A pH-Gradient Flow Cell for Converting Waste CO2 into Electricity. Environ. Sci. Technol. Lett. *4*, 49–53.
33. Toupin, M., Brousse, T., and Bélanger, D. (2004). Charge storage mechanism of MnO2 electrode used in aqueous electrochemical capacitor. Chem. Mater. *16*, 3184–3190.
34. Chen, X., Huang, G., An, C., Yao, Y., and Zhao, S. (2018). Emerging N-nitrosamines and N-nitramines from amine-based post-combustion CO2 capture–a review. Chem. Eng. J. *335*, 921–935.
35. Kanoh, H., Tang, W., Makita, Y., and Ooi, K. (1997). Electrochemical intercalation of alkali-metal ions into birnessite-type manganese oxide in aqueous solution. Langmuir *13*, 6845–6849.
36. Chen, Y.-C., Hsu, Y.-K., Lin, Y.-G., Lin, Y.-K., Horng, Y.-Y., Chen, L.-C., and Chen, K.-H. (2011). Highly flexible supercapacitors with manganese oxide nanosheet/carbon cloth electrode. Electrochim. Acta *56*, 7124–7130.
37. Nakayama, M., Konishi, S., Tagashira, H., and Ogura, K. (2005). Electrochemical synthesis of layered manganese oxides intercalated with tetraalkylammonium ions. Langmuir *21*, 354–359.
38. Simon, P., and Gogotsi, Y. (2010). Materials for electrochemical capacitors. In Nanoscience and Technology: A Collection of Reviews from Nature Journals, P. Rodgers, ed. (World Scientific), pp. 320–329.
39. Brousse, T., Toupin, M., Dugas, R., Athouël, L., Crosnier, O., and Bélanger, D. (2006). Crystalline MnO2 as possible alternatives to amorphous compounds in electrochemical supercapacitors. J. Electrochem. Soc. *153*, A2171–A2180.
40. Wei, W., Cui, X., Chen, W., and Ivey, D.G. (2011). Manganese oxide-based materials as electrochemical supercapacitor electrodes. Chem. Soc. Rev. *40*, 1697–1721.
41. Zhang, Q., Levi, M.D., Dou, Q., Lu, Y., Chai, Y., Lei, S., Ji, H., Liu, B., Bu, X., and Ma, P. (2019). The Charge Storage Mechanisms of 2D

Cation-Intercalated Manganese Oxide in Different Electrolytes. Adv. Energy Mater. *9*, 1802707.

42. Wolery, T. (2002). EQ3/6 A Software Package for Geochemical Modeling, Version 8.0, UCRL-CODE-2003-009 (Lawrence Livermore National Laboratory).

43. Newman, J., and Thomas-Alyea, K.E. (2012). Electrochemical Systems (John Wiley & Sons).

44. Toupin, M., Brousse, T., and Bélanger, D. (2002). Influence of microstucture on the charge storage properties of chemically synthesized manganese dioxide. Chem. Mater. *14*, 3946–3952.

45. Rahimi, M., Kim, T., Gorski, C.A., and Logan, B.E. (2018). A thermally regenerative ammonia battery with carbon-silver electrodes for converting low-grade waste heat to electricity. J. Power Sources *373*, 95–102.

46. Rahimi, M., D'Angelo, A., Gorski, C.A., Scialdone, O., and Logan, B.E. (2017). Electrical power production from low-grade waste heat using a thermally regenerative ethylenediamine battery. J. Power Sources *351*, 45–50.

47. Rahimi, M., Schoener, Z., Zhu, X., Zhang, F., Gorski, C.A., and Logan, B.E. (2017). Removal of copper from water using a thermally regenerative electrodeposition battery. J. Hazard. Mater. *322* (Pt B), 551–556.

Cell Reports Physical Science, Volume *1*

Supplemental Information

Carbon Dioxide Capture Using an Electrochemically Driven Proton Concentration Process

Mohammad Rahimi, Giulia Catalini, Subrahmaniam Hariharan, Miao Wang, Monica Puccini, and T. Alan Hatton

Note S1. Equilibrium speciation calculations

Potassium carbonate (K_2CO_3) was used as the absorbent with potassium chloride (KCl) as the background electrolyte; hence, the reaction system of CO_2–K–Cl–H_2O was considered in the model. All the relevant equilibrium speciation reactions are considered with the equilibrium constants tabulated in Table S1. By considering equilibrium constants (Table S1) together with the mass (Eq. S1-S3) and charge (Eq. S4) balance equations, all the speciations were calculated including CO_2 and proton activities to estimate CO_2 loading and solution pH, respectively, at different temperatures, feed gas compositions, and initial electrolyte concentrations.

Table S1. The equilibrium reactions and their corresponding constants at 50 °C of the CO_2–K–Cl–H_2O system

Equilibrium reactions	Equilibrium constants (K)	$K_{50°C}$*
$CO_{2\,(g)} \leftrightarrow CO_{2\,(aq)}$	$K_1 = \frac{a_{CO_{2\,(aq)}}}{f_{CO2}}$	1.93×10^{-2}
$CO_{2\,(aq)} + OH^- \leftrightarrow HCO_3^-{}_{(aq)}$	$K_2 = \frac{a_{HCO_3^-}}{a_{CO_{2\,(aq)}}\, a_{OH^-}}$	1.01×10^{7}
$HCO_3^-{}_{(aq)} + OH^- \leftrightarrow CO_3^{2-}{}_{(aq)}$	$K_3 = \frac{a_{CO3^{2-}}}{a_{HCO_3^-}\, a_{OH^-}}$	1.47×10^{10}
$H^+ + OH^- \leftrightarrow H_2O$	$K_4 = \frac{a_{H2O}}{a_{OH^-}\, a_{H^+}}$	1.86×10^{13}
$KCl_{(aq)} \leftrightarrow Cl^-{}_{(aq)} + K^+{}_{(aq)}$	$K_5 = \frac{a_{Cl^-}\, a_{K^+}}{a_{KCl_{(aq)}}}$	1.78×10^{2}

*data were adapted from ref.[1]

For the considered CO_2–K–Cl–H_2O system, the mass balances of the aqueous species are,

for carbon: $C_C = C_{CO_2} + C_{HCO_3^-} + C_{CO_3^{2-}}$ (S1)

for potassium: $C_K = C_{K^+} + C_{KCl(aq)}$ (S2)

for chloride: $C_{Cl} = C_{Cl^-} + C_{KCl(aq)}$ (S3)

The overall charge balance is given as:

$$\sum_i C_i z_i = 0 \tag{S4}$$

where C_i and z_i are the concentration and charge of species i, respectively. To calculate the speciation, the set of nonlinear equations given by the equilibrium reactions (Table S1), the mass balances, and the charge balance (Eq. S1-S4) was solved in MATLAB software. A comprehensive study on the gas phase, including calculations on different gas fugacities (e.g., H_2O, CO_2, and N_2) and water vapor pressure under different conditions, was also considered in the model, details of which can be found in our previous investigation.[2]

Note S2. Activity coefficients of aqueous carbon dioxide and water

The activity coefficient for CO_2 (aq) was calculated as:[2]

$$\log \gamma_{CO_2\,(aq)} = \left(C + FT + \frac{G}{T}\right)\bar{I} - (E + HT)\frac{\bar{I}}{1+\bar{I}} \tag{S5}$$

where T is the absolute temperature, $C = -1.0312$, $F = 0.0012806$, $G = 255.9$, $E = 0.4445$, and $H = -0.001606$. The activity of water was calculated as:

$$\log \gamma_{H_2O} = \frac{1}{\Omega}\left(-\frac{\sum_i C_i}{2.303} + \frac{2}{3}A_{\gamma.10}\bar{I}^{1.5}\sigma - \dot{B}\bar{I}^2\right) \tag{S6}$$

where Ω is the molar concentration of water (≈ 55.51 mol L^{-1}) and σ is given by:

$$\sigma = \frac{3}{x^3}\left(1 + x - \frac{1}{1+x} - 2\ln(1+x)\right) \quad ; \quad x = 4\,B_\gamma\sqrt{\bar{I}} \tag{S7}$$

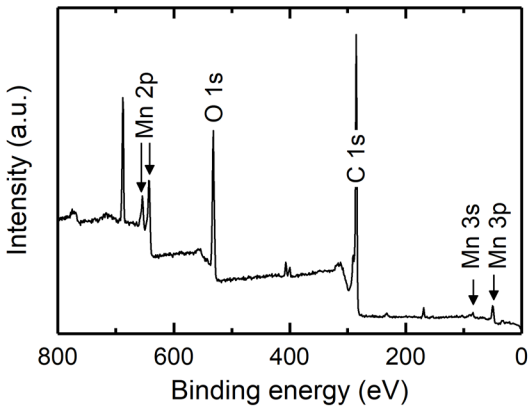

Figure S1. XPS survey spectrum of the fabricated MnO_2 electrode.

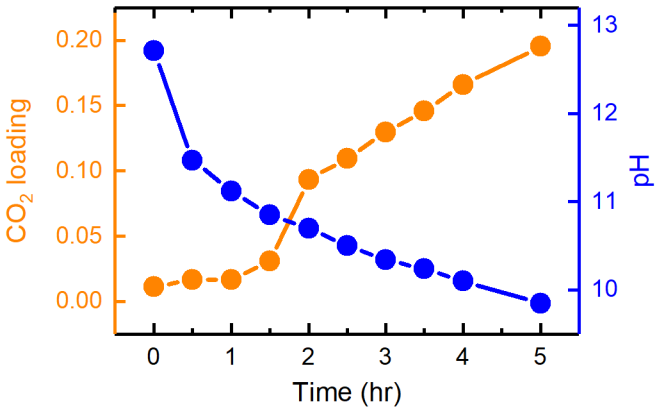

Figure S2. The kinetics of CO_2 absorption using K_2CO_3. To evaluate the absorption kinetics of CO_2, a 30% wt K_2CO_3 (similar composition to that used at the industrial scales) was purged with pure CO_2 for 5 hours at room temperature and the CO_2 loading and solution pH were measured. After 5 hours, the CO_2 loading and pH were still changing, and thus the solution needed to be purged for a longer time (e.g., overnight) to reach the equilibrium. Our measurements (not shown here) confirmed that the solution can reach an equilibrium after ~11 hours using our simple purging setup. In the future, the purging time could be significantly reduced, by for example, using a rate promoter or a purging setup with more efficient mixing system.

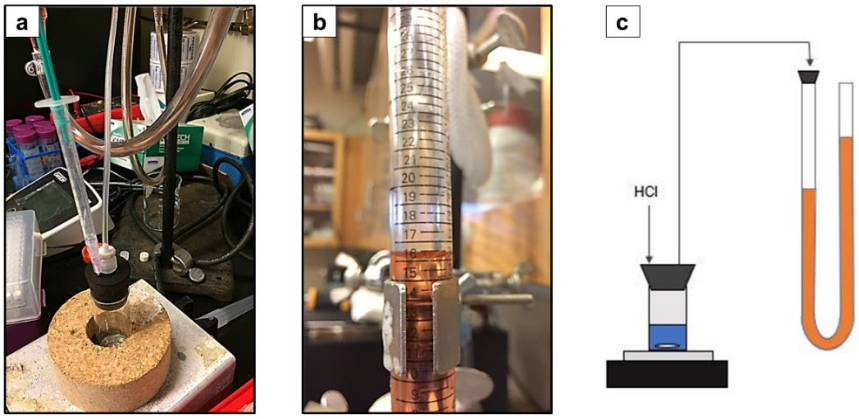

Figure S3. A CO_2 acid titration set up. (a) A sample of 1 mL of solution was mixed with 1 mL of 4 M HCl in a closed gas-tight glass vial. (b) The gas evolved was sent to a U-tube manometer to measure the increase in the volume (therefore the gas pressure) and calculate the CO_2 loading. (c) A schematic of the titration setup with a stirred reactor and a U-tube manometer.

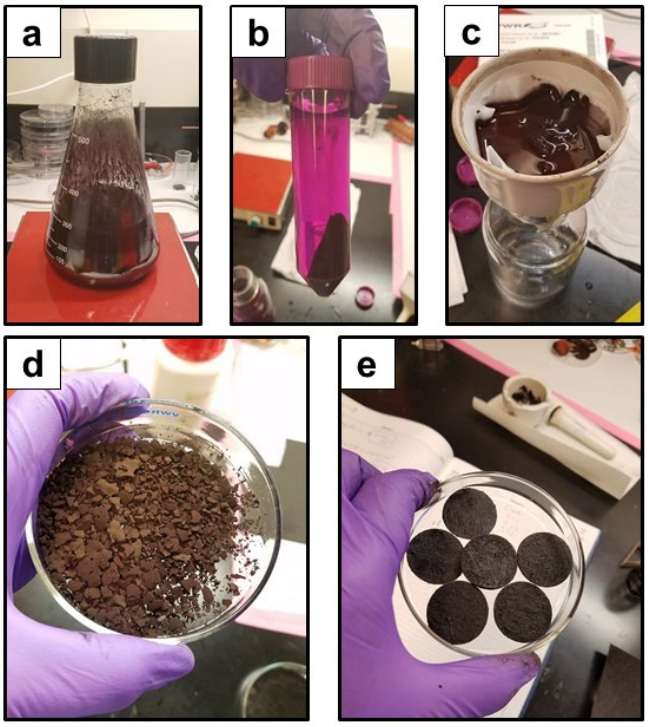

Figure S4. Fabrication of the MnO_2-based electrode using coprecipitation followed by casting on either carbon cloth or carbon felt substrate. (a) The MnO_2 precipitate was formed by mixing a 2:3 molar ratio of $KMnO_4$ and $MnSO_4$ precursors. (b) The MnO_2 precipitates were collected by centrifugation. (c) The collected precipitates were washed using deionized water and filtered. (d) The MnO_2 sample was dried overnight in a vacuum oven at 70 °C. (e) The synthesized MnO_2 powder was used to make a composite, which was later cast onto carbon cloth or carbon felt substrate.

References

1. Wolery, T. (2002). EQ3/6–Software for Geochemical Modeling Version 8.0, UCRL-CODE-2003-009.

2. Wang, M., Hariharan, S., Shaw, R.A. and Hatton, T.A. (2019). Energetics of electrochemically mediated amine regeneration process for flue gas CO2 capture. International Journal of Greenhouse Gas Control *82*, 48-58.